Speciation and Distribution of Arsenic in the Nonhyperaccumulator Macrophyte *Ceratophyllum demersum*[1][C][W]

Seema Mishra*, Gerd Wellenreuther, Jürgen Mattusch, Hans-Joachim Stärk, and Hendrik Küpper

Universität Konstanz, Mathematisch-Naturwissenschaftliche Sektion, Fachbereich Biologie, D–78457 Konstanz, Germany (S.M., H.K.); Helmholtz Centre for Environmental Research-UFZ, Department of Analytical Chemistry, D–04318 Leipzig, Germany (S.M., J.M., H.-J.S.); HASYLAB at DESY, 22603 Hamburg, Germany (G.W.); and University of South Bohemia, Faculty of Biological Sciences and Institute of Physical Biology, CZ–370 05 Ceske Budejovice, Czech Republic (H.K.)

Although arsenic (As) is a common pollutant worldwide, many questions about As metabolism in nonhyperaccumulator plants remain. Concentration- and tissue-dependent speciation and distribution of As was analyzed in the aquatic plant *Ceratophyllum demersum* to understand As metabolism in nonhyperaccumulator plants. Speciation was analyzed chromatographically (high-performance liquid chromatography-[inductively coupled plasma-mass spectrometry]-[electrospray ionization-mass spectrometry]) in whole-plant extracts and by tissue-resolution confocal x-ray absorption near-edge spectroscopy in intact shock-frozen hydrated leaves, which were also used for analyzing cellular element distribution through x-ray fluorescence. Chromatography revealed up to 20 As-containing species binding more than 60% of accumulated As. Of these, eight were identified as thiol-bound (phytochelatins [PCs], glutathione, and cysteine) species, including three newly identified complexes: Cys-As(III)-PC_2, Cys-As-$(GS)_2$, and GS-As(III)-desgly-PC_2. Confocal x-ray absorption near-edge spectroscopy showed arsenate, arsenite, As-$(GS)_3$, and As-PCs with varying ratios in various tissues. The epidermis of mature leaves contained the highest proportion of thiol (mostly PC)-bound As, while in younger leaves, a lower proportion of As was thiol bound. At higher As concentrations, the percentage of unbound arsenite increased in the vein and mesophyll of young mature leaves. At the same time, x-ray fluorescence showed an increase of total As in the vein and mesophyll but not in the epidermis of young mature leaves, while this was reversed for zinc distribution. Thus, As toxicity was correlated with a change in As distribution pattern and As species rather than a general increase in many tissues.

Arsenic (As) is ubiquitously present, considered a nonessential metalloid for plants and animals, and poses serious health hazards to humans. High levels of As in soil and drinking water have been reported around the world, with the worst situations in south and southeast Asia, where millions of people are at risk of As poisoning through drinking water and food (Chowdhury et al., 2000; Smedley and Kinniburgh, 2002; Ohno et al., 2007). Recently, As induced yield loss; thus, a threat to the sustainability of food production has been recognized as the other side of the As calamity (Brammer and Ravenscroft, 2009; Panaullah et al., 2009). Considering the enormity of As contamination, phytoremediation or the development of crops that can be grown in contaminated environments without suffering from and accumulating As in edible parts seem to be the most appropriate strategies to counter the detrimental impacts of As. These strategies demand an understanding of the mechanistic details of As uptake, toxicity, and detoxification (Tripathi et al., 2007). The in planta distribution and speciation of As are important aspects in this direction.

Inorganic arsenate [$HAsO_4^{2-}$ or As(V)] and arsenite [$H_2AsO_3^-$ or As(III)] are the most common forms of As in aquatic and terrestrial environments. Plants take up As(V) through phosphate transporters (Asher and Reay, 1979; Meharg and Macnair, 1990) and As(III) through nodulin26-like intrinsic aquaporins (Isayenkov and Maathuis, 2008; Ma et al., 2008). Inside the cell, As(V) is readily reduced to As(III) through As(V) reductase using reduced glutathione (GSH) as reductant (Duan et al., 2005; Bleeker et al., 2006). As(III) then gets complexed with thiol ligands via GSH and phytochelatins (PCs; Schmöger et al., 2000; Raab et al., 2004). Thus, complexation of As with PCs followed by sequestration of the complex in vacuoles has been suggested as the major mechanism of As detoxification in As-nonhyperaccumulator plants (Bleeker et al.,

[1] This work was supported by the Alexander von Humboldt-Stiftung (Alexander von Humboldt Fellowship to S.M.), the Deutsche Forschungsgemeinschaft (grant no. KU 1495/8), Universität Konstanz, and the Umweltforschungszentrum Leipzig.

* Address correspondence to seema_mishra2003@yahoo.co.in.

The author responsible for distribution of materials integral to the findings presented in this article in accordance with the policy described in the Instructions for Authors (www.plantphysiol.org) is: Seema Mishra (seema_mishra2003@yahoo.co.in).

[C] Some figures in this article are displayed in color online but in black and white in the print edition.

[W] The online version of this article contains Web-only data.

www.plantphysiol.org/cgi/doi/10.1104/pp.113.224303

2006; Song et al., 2010). In contrast, in hyperaccumulator plants, PCs contribute only little (1%–3%) to As complexation (Zhao et al., 2003).

An increased synthesis of PCs as well as GSH under As stress has been observed in hypertolerant (Hartley-Whitaker et al., 2001; Bleeker et al., 2003), hyperaccumulator (Zhao et al., 2003; Cai et al., 2004), as well as nonhyperaccumulator (Srivastava et al., 2007; Mishra et al., 2008, 2013) plants. However, the existence of As-PC complexation was concluded only indirectly through individual analysis of As and PCs in fractions after chromatographic separation (Sneller et al., 1999; Schmöger et al., 2000). Raab et al. (2004) for the first time showed complexes of PCs in plant extracts by using HPLC simultaneously coupled with element-specific (inductively coupled plasma-mass spectrometry [ICP-MS]) and molecule-specific (electrospray ionization-mass spectrometry [ESI-MS]) detectors. This method provides information about the diversity of ligands and As species present in plants. However, artifacts during sample preparation, such as ligand exchange for previously weakly bound metal (loids) due to the breakage of cells and subcellular compartments during the extraction of plants, cannot be excluded. In this respect, x-ray absorption spectroscopy of frozen-hydrated tissues has been proven to be a unique technique for the in situ investigation of chemical forms of metal(loids) in biological materials without much prepreparation of samples, thus minimizing the artifacts of sample preparation (Salt et al., 1995; Küpper et al., 2004). X-ray absorption near-edge spectroscopy (XANES) provides speciation of As in tissues typically by fingerprint-like comparison (if quantitative, linear combination fitting) with spectra of appropriate model compounds as standards (Pickering et al., 2000, 2006; Lombi et al., 2002, 2009; Meharg et al., 2008). Furthermore, high-resolution microscopic (μ) x-ray spectroscopy may reveal spatial distribution and speciation of As in intact biological samples (Hokura et al., 2006; Carey et al., 2010, 2011; Kopittke et al., 2012). However, species having almost identical absorption spectra cannot be distinguished by this technique, the use of inappropriate standards for fitting of experimental spectra may lead to misinterpretation, and quantification of minor contributions is always inaccurate in linear combination fitting. Studies regarding the distribution of As have been mostly done in the hyperaccumulator *Pteris vittata*, showing that the majority of As was accumulated in the pinnae, possibly in vacuoles (Lombi et al., 2002; Hokura et al., 2006; Pickering et al., 2006). In rice (*Oryza sativa*) grains, it was done with high-resolution techniques such as synchrotron-based microscopic x-ray fluorescence (μ-XRF) and secondary ion mass spectrometry by using either fractured or sectioned dry rice grains (Meharg et al., 2008; Lombi et al., 2009; Moore et al., 2010) or whole fresh rice grains (Carey et al., 2010, 2011). However, little information is available regarding the cellular or subcellular distribution of As in nonhyperaccumulator plants. Moore et al. (2011) investigated the subcellular distribution of As and silicon in rice roots through nanosecondary ion mass spectrometry. Recently, Kopittke et al. (2012) studied the spatial distribution of As in hydrated, fresh roots of cowpea (*Vigna unguiculata*) using μ-XRF including sequential computed tomography and found differences in As distribution in the plants exposed to As(V) or As(III). However, information about As speciation and distribution in leaf tissues and its relation to toxicity in nonhyperaccumulator plants is still lacking.

In this study, we analyzed the speciation (through two complementary techniques) and distribution of As in leaves of the nonhyperaccumulator submerged aquatic plant *Ceratophyllum demersum* in environmentally relevant conditions. The accumulation and speciation of As were investigated in a concentration-dependent manner at the whole-plant level in fresh extracts through HPLC-(ICP-MS)-(ESI-MS). The in situ speciation at the differential tissue level in the leaf was performed by combining high-resolution μ-XANES and confocal optics on the detector side. Using μ-XRF with full quantification including the correction of x-ray absorption in thick samples, we furthermore investigated changes in the distribution pattern of As, copper (Cu), and zinc (Zn) under sublethal to lethal As exposure in the leaves of *C. demersum*. To our best knowledge, this is the first report of As speciation in different tissues through confocal μ-XANES and of As distribution in leaves of an As nonhyperaccumulator plant. We also report direct evidence of in situ As-PC complex formation by using μ-XANES spectra of As-$(PC_2)_2$ and As-PC_3 along with As-$(GS)_3$ standards and carefully correcting for self-absorption artifacts that distorted μ-x-ray absorption spectroscopy spectra in earlier studies. Since *C. demersum* has no roots, it takes up all nutrients directly via the leaves, allowing for studies of shoot effects without interference from root uptake and root toxicity. While it is not a crop species, it is still a flowering plant (belonging to the dicotyledons) and has been accepted as a good model for laboratory studies of shoot toxicity in higher plants (Xue et al., 2012). Mechanisms of metal toxicity found in *C. demersum* are similar to other plants (Küpper et al., 1996), and like other nonaccumulator plants including crops, it detoxifies As by PCs (Mishra et al., 2008). Furthermore, it is widespread in Asia, Europe, and North America, and it has been shown to be good for removing metal from low-concentration waste water (Keskinkan et al., 2004). Additionally, its has also been used successfully in tests of biological life support systems on space flights (Blüm et al., 1994; and many articles about the Aquarack/CEBAS (for Closed Equilibrated Biological Aquatic System) and OMEGAHAB systems). Finally, the structure of *C. demersum* leaves (round, less than 1 mm diameter) makes this species a suitable model for μ-XRF and μ-XANES measurement. It facilitates the recording of whole-leaf tomograms and tissue-specific μ-XANES without any disturbance such as mixing of intercellular or intracellular fluid

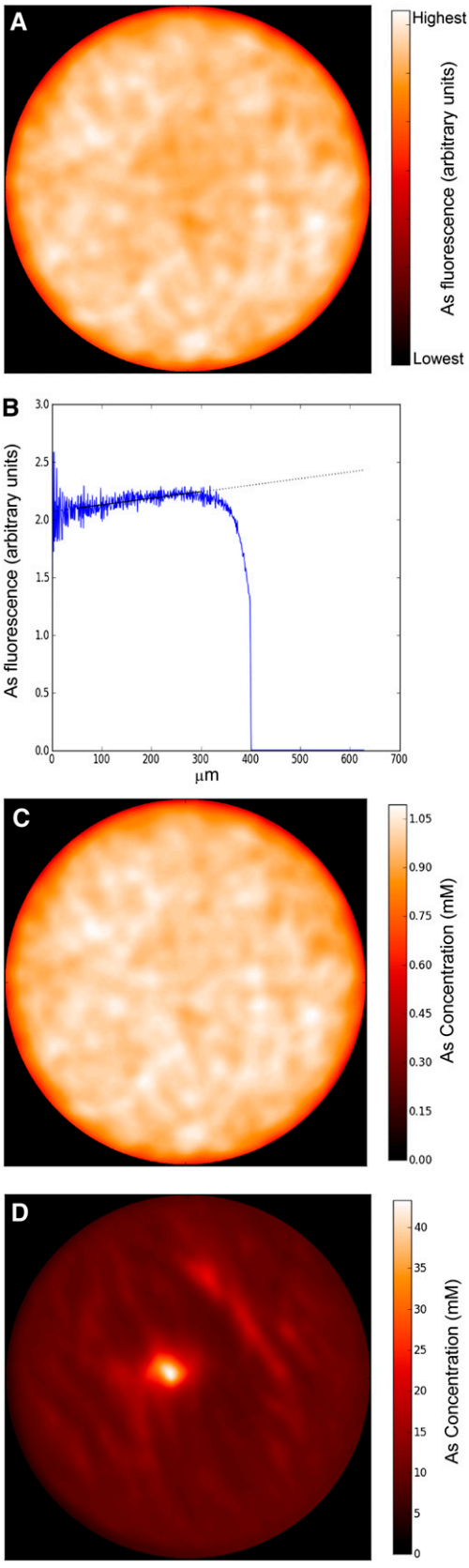

Figure 1. Method of quantitative μ-XRF used in this study. A, μ-XRF tomogram of shock-frozen (in supercooled isopentane) As standard before absorption correction. B, Absorption correction for the same standard: normalized azimuthal integration of As-K around the center of capillary. C, μ-XRF tomogram of the same shock-frozen As standard after absorption correction. D, μ-XRF tomogram of As standard frozen by immersion in liquid nitrogen. The circles contain the inner part of the capillary as obtained from evaluating the transmission of the x-ray beam (higher absorption in glass as opposed to water). [See online article for color version of this figure.]

while sectioning of the sample, thus avoiding artifacts during sample preparation.

RESULTS AND DISCUSSION

Evaluation of a New Methodology

To see the effect of freezing methods, we compared the tomograms of standards that were either shock frozen in supercooled isopentane or frozen by dipping in liquid nitrogen. In the standards frozen by immersing in liquid nitrogen, all metal(loid)s were found to be concentrated in the center of the capillary (Fig. 1D), resulting in approximately 4-fold higher concentration in the center of the capillary than in the solution. In contrast, in the shock-frozen standards, the elements were homogenously distributed (Fig. 1A). Thus, it seems that freezing by immersing in liquid nitrogen, which causes the nitrogen to boil so that heat transfer is diminished by a gas layer around the sample (known as the "Leidenfrost effect"), is not fast enough to prevent the redistribution of elements. In this way, it may also affect the distribution of elements in tissues and cause cell damage due to the formation of large ice crystals. Direct evidence concerning the preservation of intracellular compartmentation would be much more difficult to obtain. Nevertheless, inside individual cellular compartments, especially in completely liquid compartments like the vacuole, similar differences can be expected. If in the shock-frozen standard solution no rearrangement of solutes occurs, it is unlikely that such a rearrangement would happen with membranes between organelles. While these facts are generally not new, to our knowledge, the extent of this problem has never been shown before under conditions that are typical for handling biological samples. Therefore, subsequently, all the plant samples were prepared by the shock-freezing method. In this study, we used the homogeneity of our standards that were prepared in the same way and in the same sample holders as our plant samples for correcting the absorption of excitation energy and element-specific x-ray emission, which otherwise lead to an underestimation of element concentrations in the center of samples (Fig. 1). Thus, the homogeneity of standards, as found in shock-frozen samples, is also important for the correct quantification of As in leaves.

Since plant tissue contains predominantly water as a matrix, XANES of aqueous As compounds as standards are more relevant than dry salts. Furthermore,

the intensity of the white line depends on the physical state of the As, with up to 50% higher white line intensity in aqueous solutions than in powdered solid (Webb et al., 2003; Smith et al., 2005). Thus, in this study, all the standards were prepared as aqueous solutions, while in most of the earlier studies, powder of As compounds was used as a standard (Lombi et al., 2002, 2009; Meharg et al., 2008). In addition, there is a change in the intensity of the white line due to self-absorption, which increases with the concentration of the sample (i.e. it is much stronger in highly concentrated standards than in plant samples with low As concentrations). Both problems lead to inaccurate fits, from which earlier studies suffered (Lombi et al., 2002). Furthermore, the quantification results of various ligand species from XANES depend on the standards used for fitting. Therefore, the choice of the most appropriate standards is important. In most of the studies, As-$(GS)_3$ has been used as a standard for sulfur coordination in thiol-complexed As (Pickering et al., 2000, 2006; Lombi et al., 2002, 2009; Meharg et al., 2008), and some studies used As_2S_2 (Webb et al., 2003). In this study, the spectra of As(V), As(III), As-$(GS)_3$, As-$(PC_2)_2$, and As-PC_3 were used as standards (Fig. 2D). Interestingly, the spectrum of As-$(GS)_3$ was different from those of the PC complexes, but those of As-$(PC_2)_2$ and As-PC_3 were almost indistinguishable. This demonstrated that the different spatial arrangement of the ligand backbone in GSH versus PCs has an impact on the As-XANES. Beam-induced damage due to high-energy x-rays has been reported in previous studies. The most common effect is the change in oxidation state over time (Smith et al., 2005). Cooling the samples during measurement has been suggested to reduce the destructive effects of the high-energy x-rays (Parsons et al., 2002). However, despite cooling to 100 K, we found some shift in the spectra of As(III) toward higher energy over time (if more than three scans were measured at the same position; data not shown). Therefore, for each scan, the sample was moved by 2 μm along the axis of the standard or leaf.

By the combination of μ beam size (800 nm) and confocal detector optics, it was possible to distinguish between different tissues. To our knowledge, this is the first application of confocal optics in μ-XANES of plant tissues. Figure 2A shows that the confocal optics worked well, and we could measure epidermis, mesophyll, and vein tissues (including xylem, phloem,

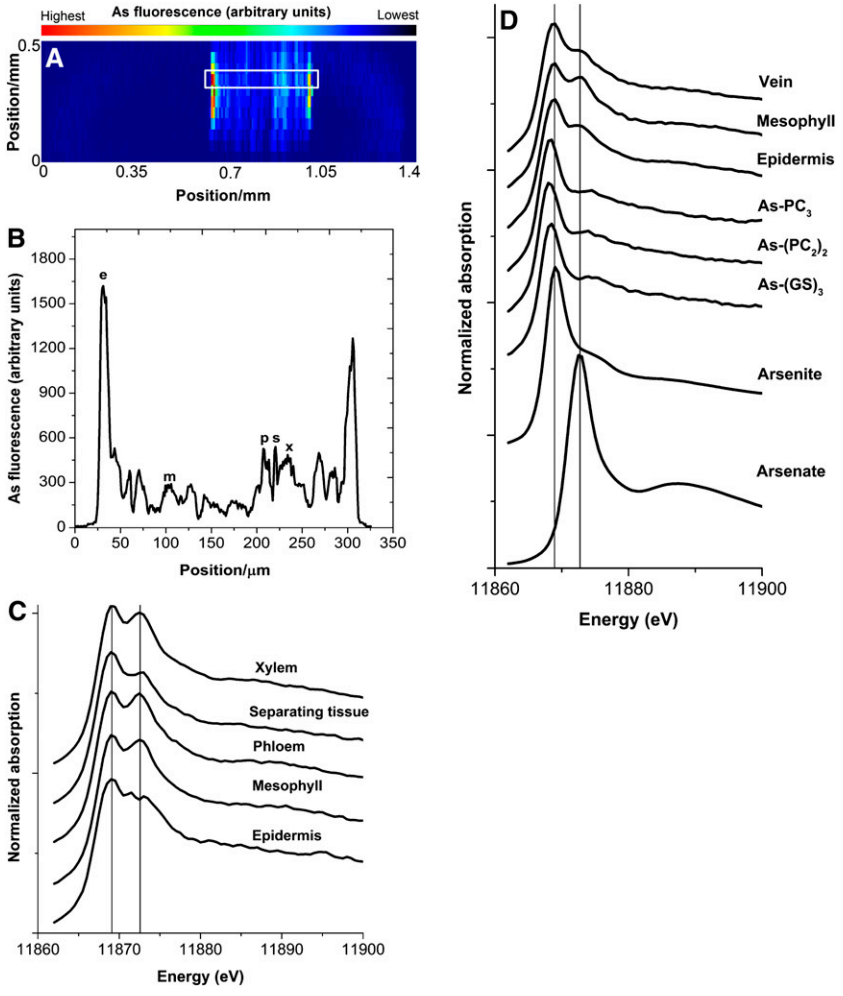

Figure 2. Method of μ-XANES used in this study. A, 2D map of a young mature leaf, exposed to 1 μM As, showing selected positions for epidermis, mesophyll, and vein. Note that resolution in the direction of the beam was limited to about 130 μm by the confocal optics, in contrast to the resolution orthogonal to the beam, which was limited by the beam size of 0.8 μm. For this reason, for the 2D map, a step size of 50 μm in the direction of the beam (y direction) was chosen, while horizontally, a step size of 5.5 μm was chosen for fast measurement. B, Fine sweep (1-μm horizontal resolution) of selected transects through the leaf showing the points of measurements. e, Epidermis; m, mesophyll; p, phloem; s, separating tissue; x, xylem. C, μ-XANES spectra of selected tissues in fine sweep. D, μ-XANES spectra of standards and 5 μM As-exposed mature leaf. [See online article for color version of this figure.]

and separating tissue in between; Fig. 2, A–C) without cross contamination of other tissue signals by the epidermis, despite a high concentration of As in the epidermis. On this basis, in the future, it will be possible to analyze the spatial heterogeneity of metal(loid) speciation in many tissues that are difficult to separate physically without artifacts. As the signal in the vein and epidermis was much higher than in the mesophyll (Fig. 2, A and B; discussed in detail below), contamination of the vein signals by the mesophyll remained small, although these tissues extend less in the *z* direction (i.e. along the axis of the beam) than the confocal optics can separate (about 130 μm). Since the mesophyll was thicker than the 130-μm optical depth of the confocal measurement, speciation in this tissue also could be analyzed despite the fact that it contains far less As than the epidermis surrounding it. Focusing on different tissues in the vein, however, needed several two-dimensional (2D) maps at different angles to find the position showing all tissues (phloem, xylem, and separating tissue in between). Therefore, due to the limitation of beam time in most of the samples, differentiation in the vein had to be skipped and only the whole vein was measured.

Uptake and Distribution of As, Cu, and Zn in *C. demersum*

Plants showed significant accumulation of As on a whole-plant basis ($P = 0.004$) determined in digested fresh tissue (Fig. 3). Due to the limitation of beam time at synchrotrons, the distribution study (through μ-XRF) of As and two important micronutrients, Cu and Zn, was done at only two As concentrations (1 and 5 μM As) in young mature leaves and at 5 μM As in mature leaves (Fig. 4). The concentrations were chosen on the basis of the effect on plant growth (Supplemental Fig. S1). The tomographic reconstruction of the μ-XRF measurements showed that at 1 μM As, most of the accumulated As was concentrated in the epidermis, where concentrations ranged from 1.5 to 3 mM (i.e. up to 3,000-fold higher than in the nutrient solution). A slightly lower concentration, around 1.5 mM, was accumulated in the vein, and the least (less than 0.05 mM; i.e. close to the background level in the control) was found in the mesophyll of young mature leaves. However, upon exposure to 5 μM As, the level of As in the epidermis did not show a further increase, while in the vein, it increased drastically (up to 4.5 mM). Moreover, at this concentration, a considerable level (around 2 mM) of As was also observed in mesophyll cells of young mature leaves. In mature leaves, in contrast, at this concentration, the level of As sequestered to the epidermis increased drastically (up to 7 mM), while its level in the vein did not show any further increase and there were no measurable amounts of As in the mesophyll (Fig. 4).

Cu was mainly localized in the vein, and its level in the vein did not show any considerable change upon As exposure in both young mature and mature leaves

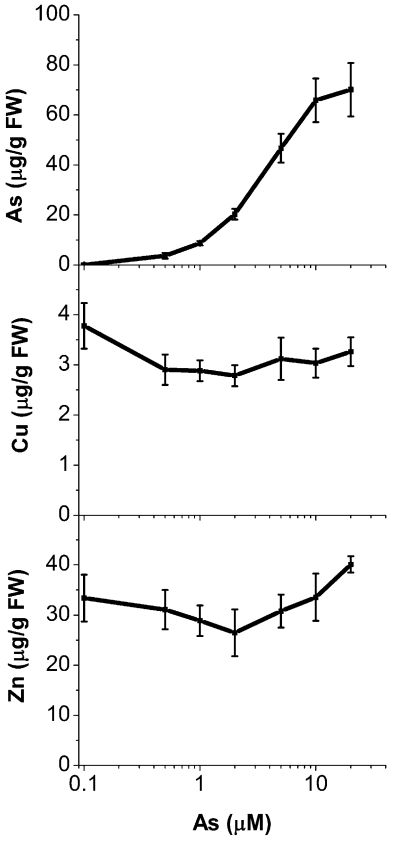

Figure 3. Accumulation of As, Cu, and Zn in plants exposed to different concentrations of As for 15 d. Data ± SD, $n = 9$. FW, Fresh weight.

(Fig. 4). On a whole-plant basis as measured by ICP-MS analyses of the digested tissues, Cu accumulation decreased slightly ($P = 0.113$ [not significant at $P = 0.05$]), particularly at lower As (0.5, 1, and 2 μM; Fig. 3).

In contrast to Cu, Zn was homogenously distributed over the whole leaf in control plants, but the distribution pattern of Zn changed upon As exposure. With an increase in As concentration, Zn was located more in the epidermis (Fig. 4). At 5 μM As, the greatest proportion of Zn was located in epidermis of both young mature (0.35–0.7 mM) and mature leaves, with higher concentrations in mature leaves (up to 0.85 mM). The concentration of Zn in the plants did not change significantly ($P = 0.096$ [not significant at $P = 0.05$]) up to 2 μM As, and beyond that it increased higher than the control as measured by ICP-MS in the digested fresh tissues (Fig. 3).

From net growth rate, it was evident that already at 1 μM, As plants experienced some toxicity; at 5 μM As, net growth was about zero (Supplemental Fig. S1). Therefore, we termed these concentrations sublethal and lethal, respectively. At the sublethal concentration, As was mostly sequestered in the epidermis of young mature leaves. This is a compartmentation pattern that had been found also for the As hyperaccumulator

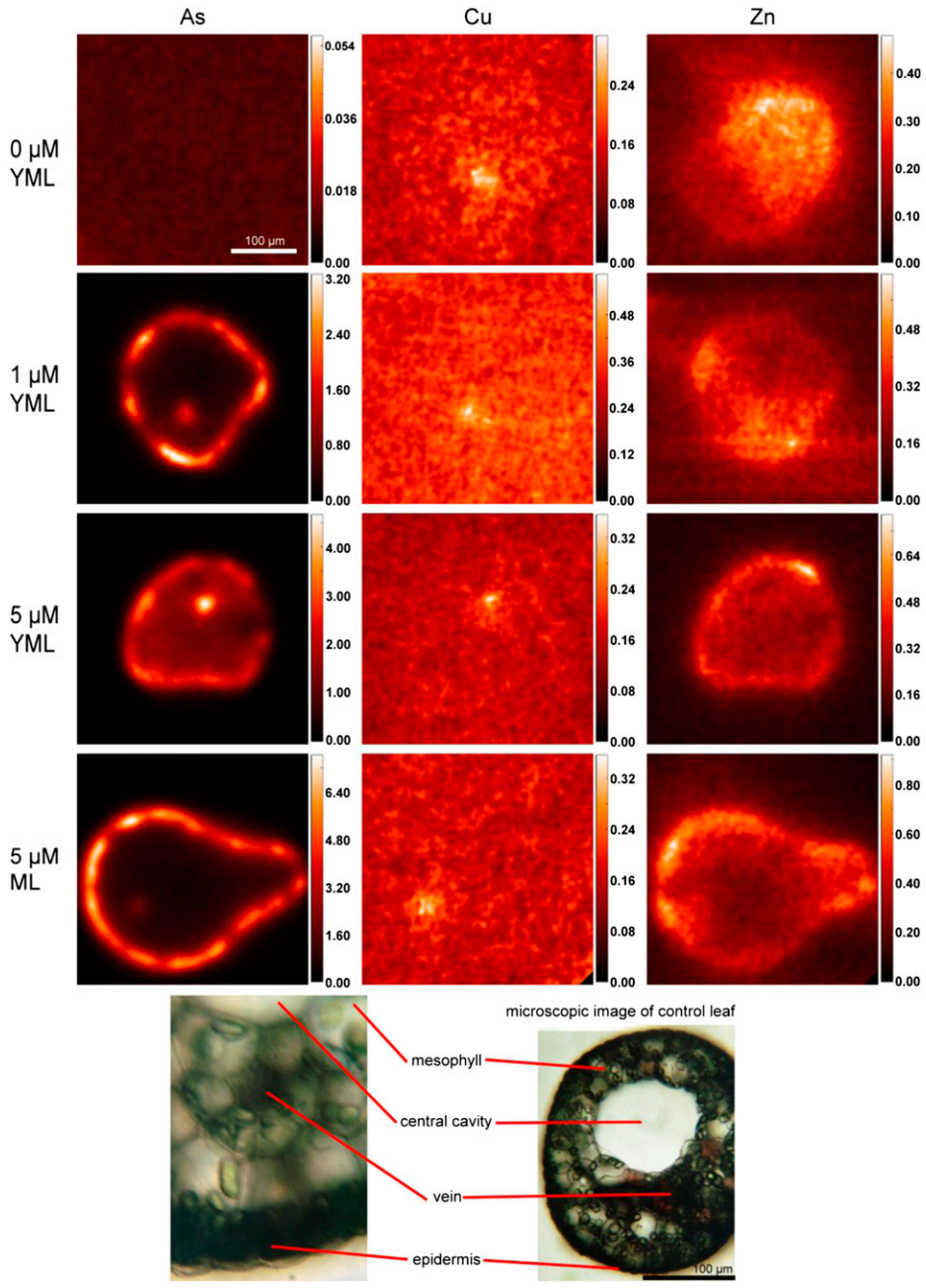

Figure 4. X-ray fluorescence microtomograms showing As, Cu, and Zn distribution in leaves of *C. demersum* after 2 weeks of growth in control conditions or exposed to As. For all samples, at least two replicate leaves from two separate As treatment experiments were measured, and representative examples are shown. Scale bars at right represent millimolar concentrations of elements. ML, Mature leaf; YML, young mature leaf. [See online article for color version of this figure.]

P. vittata (Lombi et al., 2002) and various other metal hyperaccumulators (Küpper et al., 1999, 2001). At the lethal concentration, a considerable accumulation of As occurred in mesophyll cells, and As in the vein further increased, while the levels of As in the epidermis were comparable at both sublethal and lethal concentrations. It seems that the epidermal cells sequestered As to their maximum capacity already at the sublethal concentration, and any further accumulated As started to distribute in other tissues like the mesophyll. Since the mesophyll is the photosynthetically most active tissue, an increase in concentration of As in this tissue may damage photosynthetic pigments and, subsequently, photosynthesis as well. The drastically increased As in the vein at this concentration indicates that the As coming through the vein could not be distributed to the surrounding tissues, either due to a disturbance in transporter activity or to limited As accumulation capacity of mesophyll cells in young mature leaves. This accumulation in the vein is particularly remarkable because *C. demersum* has, due to its aquatic lifestyle, reduced conductive tissues, and in principle nutrients may reach the leaf mesophyll not only by import through veins but also directly through the epidermis. In this way, the increase in the level of Zn in the epidermis at the lethal concentration may

Table I. *As complexes, molecular masses, and retention times after HPLC-(ICP-MS)-(ESI-MS) of synthesized standards*

As Complexes	*m/z*	Retention Times
		min
Cys-$As^{(III)}$-desgly-PC_2	675/338	5.1
Cys-As-$(GS)_2$	808/404.5	5.95
PC_2-$As^{(III)}$(OH)	630	7.35
Cys-$As^{(III)}$-PC_2	733/367	7.96
$As^{(III)}$-$(GS)_3$	994/497.5	12.43
GS-$As^{(III)}$-desgly-PC_2	862/431.5	16.86
GS-$As^{(III)}$-PC_2	919/460	17.96
As-PC_3	844/422.5	20.34
$MA^{(III)}$-PC_2	628/314.5	21.5
As-$(PC_2)_2$	1,151/576	22.4 and 23.7

also be attributed to a disturbance in Zn transporters. In mature leaves, epidermal cells showed a noticeably higher capacity of As sequestration compared with young mature leaves, probably because of bigger vacuoles; thus, in these leaves even at the lethal concentration, the level of As in mesophyll and vein remained low. Furthermore, the increase in the level of micronutrients, especially Zn, at higher As concentration observed at the whole-plant level could be related to changes in their distribution. Since at higher As most of the Zn was sequestered to the epidermis, mesophyll cells probably were short of Zn and enhanced Zn transport. Such an effect for Cu could not be clear because of its low concentration in the plant.

Speciation of As in *C. demersum*

In this study, chromatographic analysis of plant extracts and spectroscopic analysis in intact tissues complemented each other. Chromatography is fully quantitative and much more powerful in distinguishing between various different thiol ligands that have similar or even identical XANES spectra (in particular, all the variants of PCs), while XANES of frozen-hydrated tissues allows analysis without extraction artifacts and comparison of speciation between different tissues that would be mixed by extraction.

As Speciation at the Whole-Plant Level in Extracts of As-Exposed Plants through HPLC-(ICP-MS)-(ESI-MS)

As speciation at the whole-plant level was done at all exposure concentrations (i.e. 0–20 μM As in the nutrient solution). The molecular masses (mass-to-charge ratio [*m/z*] for $[M+H]^+$ and $[M+2H]^{2+}$) and retention times of various As complexes synthesized from standards are given in Table I. Chromatographic separation of fresh extracts from As-exposed plants is shown in Figure 5. The extraction efficiency of As was 89% ± 6.3% (n = 42), and the chromatographic recovery of As was 92% ± 9.2%.

The ICP-MS (*m/z* 75 As) data after chromatography showed up to 20 As species, of which eight were identified (Fig. 5). The identification of six species, PC_2-$As^{(III)}$(OH), Cys-$As^{(III)}$-PC_2, GS-$As^{(III)}$-desgly-PC_2, GS-$As^{(III)}$-PC_2, $As^{(III)}$-PC_3, and $As^{(III)}$-$(PC_2)_2$, was carried out by their characteristic retention times and characteristic *m/z* peaks in ESI-MS as identified for standard complexes (Table I). As(III)-$(PC_2)_2$ showed two peaks at 22.4 and 23.7 min in ICP-MS (*m/z* 75 As) and corresponding *m/z* signals in ESI-MS. These are probably isomers having different log octanol/water partition coefficients reflecting the difference in polarity and retention times as well. The 1-octanol-water coefficient was calculated based on the software Molecular Modeling Pro (ChemSW) for personal computers (data not shown). The peaks at 6.5 and 21.5 min were identified as Cys-As-$(GS)_2$ and monomethylarsonic

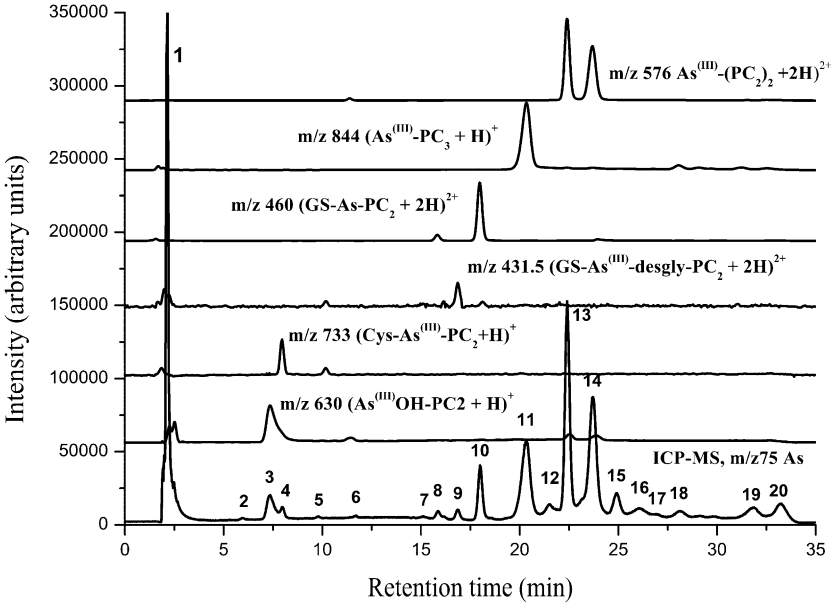

Figure 5. Chromatogram of As species in *C. demersum* exposed to 20 μM As(V) for 15 d. HPLC was coupled to ICP-MS (*m/z* 75 As) and simultaneous ESI-MS (*m/z* 576, 844, 460, 431.5, 733, and 630). Peak 1 contains inorganic As(III) and As(V); peak 2 contains Cys-As-$(GS)_2$; peak 3 contains $As^{(III)}$(OH)-PC_2; peak 4 contains Cys-$As^{(III)}$-PC_2; peak 9 contains GS-$As^{(III)}$-desgly-PC_2; peak 10 contains GS-$As^{(III)}$-PC_2; peak 11 contained $As^{(III)}$-PC_3; peak 12 contains monomethylarsonic PC-2 [$MA^{(III)}$-PC_2; CH_3As-(γ-Glu-Cys)$_2$-Gly]; and peaks 13 and 14 contain As(III)-$(PC_2)_2$. All other peaks are yet unidentified As species.

PC-2 [$MA^{(III)}$-PC_2; CH_3As-(γ-Glu-Cys)$_2$-Gly], respectively, by comparing the retention times of the standards (Table I), because their *m/z* signals in As(V)-exposed plant extracts were too small. The speciation of As through anion-exchange chromatography showed traces of monomethylarsonic acid along with As(V) and As(III), with As(III) being the predominant species (approximately 83%–90%), while no dimethylarsinic acid was detected (Supplemental Fig. S2).

Concentration-dependent analysis of complexes showed that at all concentrations, a significant amount of As was eluted as unbound inorganic As (Fig. 6A; approximately 36% ± 4.6%). Among the complexed As, GS-$As^{(III)}$-PC_2, $As^{(III)}$-PC_3, and $As^{(III)}$-$(PC_2)_2$ contributed most at all concentrations (i.e. up to 12%, 18%, and 42% of the total bound As at 20 μM). However, their contribution differed depending on As exposure concentration (Fig. 6). At lower concentrations up to 1 μM As, the contribution of GS-$As^{(III)}$-PC_2 and $As^{(III)}$-PC_3 was higher in comparison with $As^{(III)}$-$(PC_2)_2$, while at higher As concentrations, the contribution of $As^{(III)}$-$(PC_2)_2$ increased significantly ($P < 0.001$). Also, the level of other identified As species increased slightly, and the total level of several yet unidentified species increased significantly ($P < 0.001$; Fig. 6A) with increases in As concentration; however, their contribution to total bound As decreased (Fig. 6B). Unbound thiols (Cys, reduced and oxidized GSH, PC_2, and PC_3) were

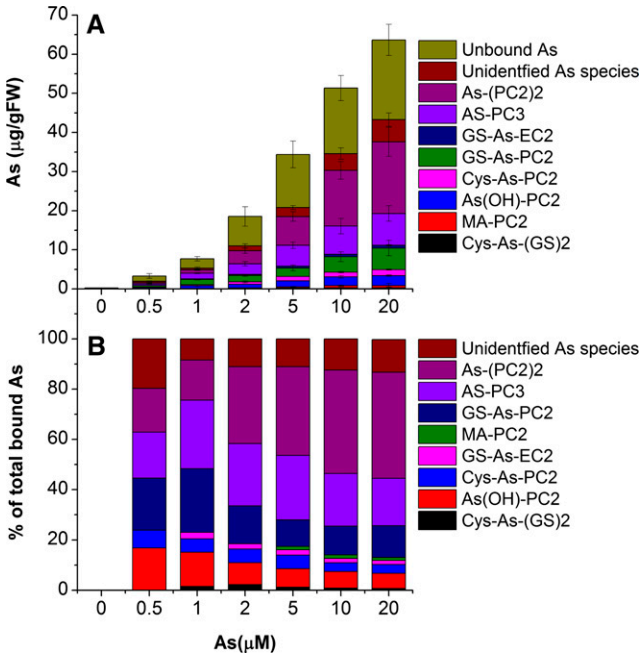

Figure 6. Quantitative determination of As species analyzed through HPLC-(ICP-MS)-(ESI-MS). A, As species (*m/z* 75) in *C. demersum* exposed to various concentrations of As for 15 d. Data ± SD, $n = 9$. FW, Fresh weight. B, Percentage contribution of different As species to total bound As at different exposure concentrations. [See online article for color version of this figure.]

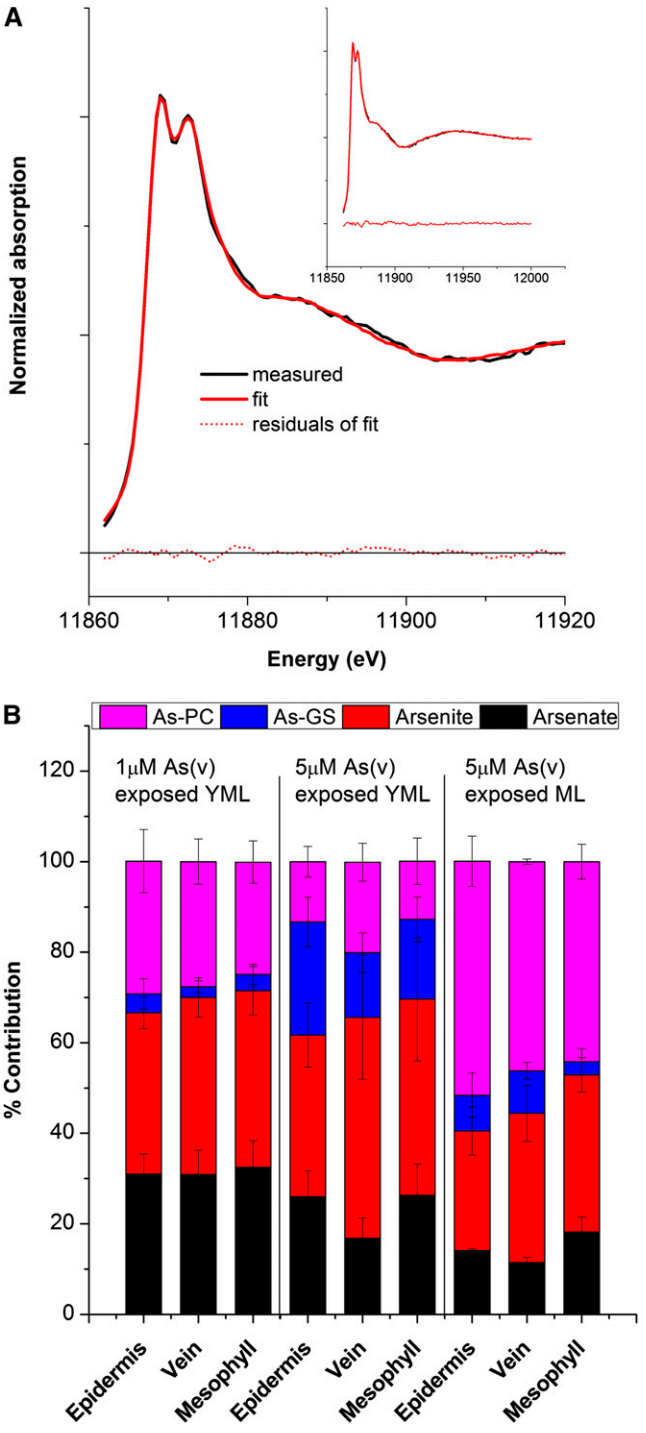

Figure 7. Quantitative analysis of confocal μ-XANES in various tissues. A, Fit quality of the spectra of epidermis of a young mature leaf. B, Quantitative data showing the percentage contribution of different As species in various tissues of young mature leaves (YML) and mature leaves (ML). Two replicate leaves from two separate As treatment experiments were measured. [See online article for color version of this figure.]

also identified in ESI-MS (data not shown), while no free PC_4 or PC_4-containing As species were detected at any As concentration. This was in agreement with previous studies in *C. demersum*, which showed induction of PC_2 and PC_3 in response to As and other heavy metals (Mishra et al., 2006, 2008, 2009).

These results show that PCs play an important role in As detoxification in *C. demersum*, complexing up to 68% of total eluted (about 56% of total accumulated) As, which is significantly higher than in other non-hyperaccumulator plants (Raab et al., 2005; Srivastava et al., 2007) and also higher than in *C. demersum* in a previous study (Mishra et al., 2008). Chromatography showed considerable diversity in As species, including novel Cys-containing As species. However, the physiological importance of various minor identified and unidentified species is not clear. Although the complexation and ligand exchange of weakly bound As during extraction may not be excluded, it seems unlikely to be a reason for the existence of cysteine- and GSH-containing As complexes, because the levels of cysteine and GSH in whole-plant extract were far lower than PC_2 (data not shown). The in vitro complexation of As by purified thiols during the preparation of standards showed the complexation efficiency in the order $PC_3 > PC_2 > GSH > Cys$. Probably, these minor species are intermediates before stabilized As-PC complexes are formed, or they are synthesized in tissues having less PC synthase activity. As-PC_3 is the preferential complex in cellular conditions, as found in *Holcus lanatus* and sunflower (*Helianthus annuus*), because it has a more stable trihedral coordination with three –SH groups than GS-$As^{(III)}$-PC_2 or $As^{(III)}$-$(PC_2)_2$ (Raab et al., 2004, 2005). However, in this study, at higher concentrations, the percentage complexation of As-PC_3 decreased, probably due to the insufficiency of PC synthase activity to form long-chain PCs.

In Situ Speciation of As through Confocal μ-XANES in Intact Frozen Hydrated Samples

The speciation of As through μ-XANES was done in the same samples that had previously been used for μ-XRF measurements (i.e. in leaves exposed to 1 or 5 μM As), so that distribution and speciation could be directly compared. Selected μ-XANES spectra from different tissues (epidermis, vein, and mesophyll) of a leaf, as well as the spectra of standards, are reported in Figure 2, C and D. The fit of the spectra of epidermis of young mature and mature leaves is shown in Figure 7A and Supplemental Figure S3 as examples.

Since the spectra of As-$(PC_2)_2$ and As-PC_3 were identical, these species were fitted as a single contribution in the quantification of As species. The μ-XANES results revealed that around 40% to 70% of As was unbound inorganic As, with a higher proportion of As(III) than As(V) in all measurements (Fig. 7). However, this proportion strongly varied depending on tissue type, leaf age, and As exposure concentration, showing more free As in the young mature leaves exposed to 1 μM As than those exposed to 5 μM As, and the least in the mature leaf exposed to 5 μM As. Furthermore, a greater proportion of free As was found in the mesophyll and the least in the epidermis of all samples. Among thiol-bound As, most of the As was found to be coordinated with PCs both in 1 μM As-exposed young mature leaves and in the 5 μM As-exposed mature leaf. However, young mature leaves exposed to 5 μM As showed a relatively high proportion of GSH-bound As. Furthermore, in young mature leaves, when the As exposure concentration was increased from 1 to 5 μM, thiol-bound As increased in all tissues. Additionally, in the vein and mesophyll, the proportion of free As(III) was increased over As(V). It seems that at high influx of As in young mature leaf, most of the As(V) was reduced to As(III) and GSH

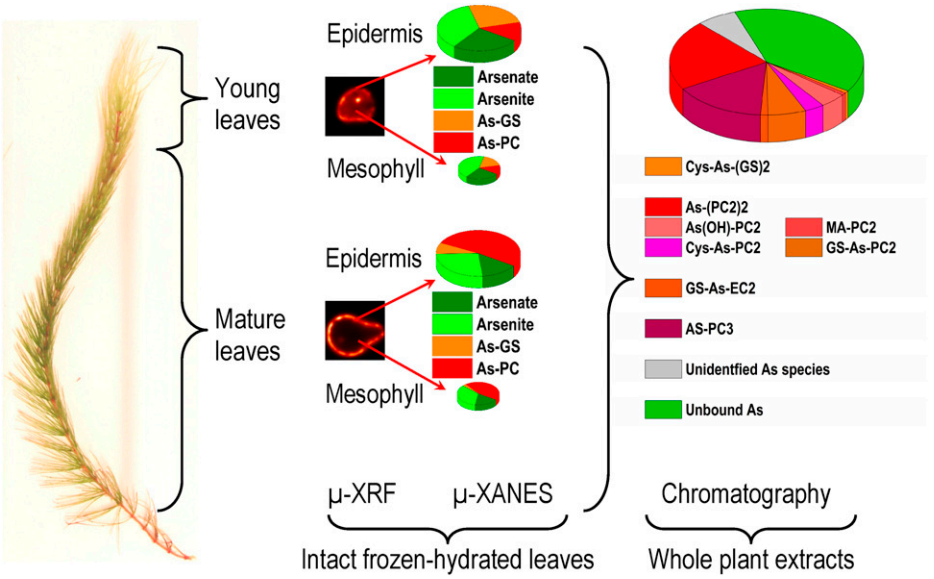

Figure 8. Correlation of the different approaches of investigating As speciation and distribution in this study. The data shown were taken from measurements at 5 μM As. [See online article for color version of this figure.]

served as the first available ligand, but due to the limited storage capacity of the epidermis, a considerable amount of the As(III), including thiol-bound As (III), was accumulated in the vein and also in the mesophyll. This was also evident by the distribution measured via μ-XRF.

Since μ-XANES provides relative speciation within measured tissues, the detailed interpretation of these results needs to consider the difference in the level of total As in each tissue type as revealed by quantitative μ-XRF maps. At first glance, it appears that μ-XANES showed lower thiol-bound As in intact tissues than chromatography at the whole-plant level. This may occur due to ligand exchange of weakly bound As during extraction. Nevertheless, when relative contributions of tissues (i.e. young mature versus mature leaves [1:3]) with the concentration of As in each tissue (approximately 2- and 14-fold higher As concentration in epidermis than in mesophyll of young mature and mature leaf, respectively) were taken together into account, the results of both techniques were comparable (Fig. 8). From μ-XRF maps, it is evident that most of the As was localized in the epidermis and the maximum level of As was in the epidermis of mature leaf. Furthermore, the mature leaf contained up to 60% thiol-coordinated As. Thus, considering the higher contribution of mature leaves in total As on the whole-plant level, the results of XANES are in agreement with the chromatographic speciation results, which showed about 59% thiol-bound As at 5 μM As in the nutrient solution (Fig. 8). The active reduction of most of the As(V) to As(III) in all tissues and the increase in the level of complexes with increases in the As concentration showed that the As(V) reductase and GSH metabolism, and thus PC synthesis, were not inhibited at the whole-plant level. Nevertheless, in young mature leaves at high As concentration, the rate of PC synthesis might be limiting, leading to an increase in GSH-bound As in the epidermis and free As(III) in other tissue as revealed by the XANES data. Furthermore, although the proportion of unbound As was not increased by an increase in As concentration, the total amount increased and spread to the physiologically more active tissue (i.e. mesophyll), leading to toxicity.

CONCLUSION

The speciation of As through two complementary methods along with As distribution in *C. demersum*, to our knowledge, is the most comprehensive study up to now, which has revealed that in plants there is considerable diversity in ligands for As complexation. The level of complexed As increased with increases in As concentration, up to 60% of total accumulated As. The changes in the distribution of As from epidermis to mesophyll tissue from sublethal to lethal As concentration, as depicted by μ-XRF measurements, could directly be related to the toxicity experienced by the plants. Furthermore, the first tissue-specific As speciation at different concentrations of As and ages of tissues revealed that the increased level of As in mesophyll at these concentrations was mostly free As(III). This study demonstrated that As not only affects the uptake of nutrients but also changes their distribution pattern, as depicted by the Zn distribution μ-XRF maps. This may lead to As-induced Zn deficiency in the mesophyll. The μ-XANES coupled with confocal optics has shown new possibilities for the detailed investigation of tissue-specific differences in metal(loid) ligands even up to different vascular tissues.

MATERIALS AND METHODS

Plant Material and Cultivation

Ceratophyllum demersum plants were grown in nutrient solution that was optimized for submerged macrophytes (final concentrations listed in Supplemental Table S1). The nutrient solution was aerated continuously and constantly exchanged by peristaltic pumps at a rate of 0.4 mL min^{-1}, with 2-L resident volume. The temperature and light conditions were 14-h daylength, 24°C day/20°C night temperatures, and a sinusoidal light cycle with maximum irradiance of approximately 100 μmol m^{-2} s^{-1} supplied by "daylight" fluorescent tubes (Dulux L 55 W/12-950; Osram).

For the experiments, plants of similar weight (approximately 1 g) were chosen and exposed to As (0–20 μM) prepared in nutrient solution by using the salt Na_2HAsO_4 (Alfa Aesar). Although As was provided as As(V), it is known that in solution it becomes a mixture of As(V) and As(III) due to efflux from plants (Xu et al., 2007; Xue et al., 2012). Therefore, in the following, we only use the label "As" for this mixture of redox states. Each aquarium contained one plant, and an aquarium without As served as a control. To minimize variations in biomass-media ratio over the course of the experiment, the plants were cut weekly to the fresh weight of the plant having the lowest growth rate.

Elemental Analyses

Total As, Cu, and Zn were measured in fresh plant material after acid digestion (HNO_3-H_2O_2 in a microwave digester). Element concentrations were analyzed using a sector field inductively coupled plasma mass spectrometer (Element XR; Thermo Fisher Scientific). Prior to analysis, ICP-MS parameters were optimized every day, and the calibration was verified using the following reference materials: SLRS-5 (River Water Reference Material for Trace Metals; National Research Council Canada), SPSSW1 (Surface Water Level 1; Spectra Pure Standards), and SRM 1643e (Trace Elements in Water; National Institute of Standards and Technology). An addition of rhodium (4 μg L^{-1}) to all samples was used for internal standardization.

Sample Preparation

Sample Preparation for As Speciation through Chromatography

Plant Extracts. Plants were harvested and rinsed in ice-cold 2 mM phosphate buffer (pH 6.0) for 15 min followed twice by ice-cold deionized water for 2 min and shaken to remove surface water. Plants were immediately frozen and ground in liquid nitrogen and aliquoted (300–500 mg) in precooled and weighed microfuge tubes. An aliquot was immediately extracted in 1% (v/v) degassed formic acid (plant material:liquid ratio of 1:2, 90 min at 1°C), centrifuged for 5 min at 1°C, and extract was quickly transferred to a sample vial and kept at 4°C in the HPLC autosampler for the determination of As-PC complex. Total As was also determined in the same extract. Other subsamples were digested for the determination of total accumulation by the plant and for the determination of extraction efficiency by ICP-MS as mentioned above.

Standards. Standards of PC (90%–95% pure PC_2, PC_3, PC_4, desgly-PC_2 [PC_2 without the C-terminal Gly], and desgly-PC_3 [in 6.3 mM diethylenetriaminepentaacetic acid/0.1% trifluoroacetic acid]) procured from Clonestar Peptide Services were used for synthesizing various standards of As-thiol complexes

and applied to HPLC-(ESI-MS)-(ICP-MS). The retention times and characteristic *m/z* values of standards (Table I) were used for the identification of complexes in plant extracts. For synthesizing the complexes, reaction mixtures [5 mM As (III), 200 μM each PC and/or 2 mM GSH, and 10 mM Cys] were prepared in 0.1% degassed formic acid under nitrogen and kept overnight under nitrogen.

Sample Preparation for Synchrotron-Based As Speciation and Elemental Mapping

Frozen-Hydrated Plant Samples. For synchrotron-based measurements, 2 and 5 μM As-exposed plants were washed thoroughly with nutrient solution without micronutrients and As. One fully developed leaf from the fourth to fifth whorl and one from the 15th to 16th whorl (counted from the tip) were sampled and termed as young mature leaf and mature leaf, respectively. For sample preparation, ultraclean glass capillaries (1-mm diameter, 0.1-mm wall; Hilgenberg) were cut to adequate size and filled with water. The leaf was inserted into the water-filled capillary with caution to avoid any damage to the leaf; subsequently, the filled capillary was fixed on a custom-made sample holder. The capillaries containing leaves were immediately shock frozen in supercooled isopentane (−140°C) and stored in liquid nitrogen until the analysis.

Standards. For calibration of μ-XRF tomograms, a multielement standard containing 1 mM each of Na_2HAsO_4, $CdCl_2$, $CrCl_3$, $CuCl_2$, NaFe(III)-EDTA, $NiCl_2$, and $ZnCl_2$ in 20% glycerol + 5% HCl (final concentrations) was diluted from stock solutions and filled into the same capillaries as used for the leaves. For comparison of freezing methods, two kinds of standards were prepared: one was shock frozen like the plant samples (Fig. 1A) and the other was frozen by immersing in liquid nitrogen (Fig. 1D).

To determine the speciation of As through μ-XANES, the following standard reference compound solutions were prepared. Complexes of As with GSH [1.5 mM As(III) and 65 mM GSH], PC_2 [0.8 mM As(III) and 3.5 mM PC_2], and PC_3 [1 mM As(III) and 2.7 mM PC_3] were prepared. For complexation, the reaction mixtures were kept under nitrogen for either 30 min or overnight for reaction and were frozen in capillaries as mentioned above.

Instrumental Setup and Measurements

Chromatographic and Detector Conditions

For the separation and identification of the As species present in fresh plant extracts, HPLC coupled to ESI-MS (molecule-specific detector) and ICP-MS (element-specific detector) was used. The HPLC and detector conditions were according to Raab et al. (2004) with slight modifications. Briefly, an Atlantis reverse-phase C18 analytical column (4.6 × 150 mm, 5-μm particle size; Waters) was used for the separation of As-PC complexes on a 1100 Series HPLC system (Agilent Technologies). A gradient of 0.1% (v/v) formic acid (A) and 0.1% formic acid in 20% (v/v) methanol (B) was used (0–20 min, 0%–75% B; 20–30 min, 75% methanol; 30–30.10 min, 20%–0% B; 30.10–35 min, 0% B). Postcolumn, the flow was split in a ratio of 1:1 into the ICP-MS and ESI-MS devices. ESI-MS (6130 quadrupole LC/MSD; Agilent Technologies) was used in the positive ionization mode from *m/z* 120 to 1,200 or in the single ion monitoring mode with the electrospray ionization source. For the identification of As species, the characteristic retention time and *m/z* ratio in ESI-MS along with trace As (*m/z* 75) at the corresponding retention in ICP-MS (7500ce; Agilent Technologies) was applied. For the quantification of As species, only ICP-MS data (*m/z* 75) were used. Dimethylarsinic acid was used as a standard for the calibration and quantification of all As species.

Instrumental Setup for Synchrotron-Based Spectroscopy and Elemental Mapping

All μ-XRF measurements were done at beamline L of the synchrotron DORIS at the Deutsches Elektronen Synchrotron (DESY). X-rays created in a bending magnet were monochromatized using a multilayer monochromator at 15 keV with approximately 2.3% band pass. Focusing was achieved using a single-bounce capillary to approximately 10-μm spot size in both horizontal and vertical dimensions. To limit beam damage, throughout the measurement the sample was cooled in a cryostream from top to about 100 K (Cryocool LN3; Cryoindustries of America). μ-XRF tomography was done approximately 3 mm above the branching point of the leaf with step size of 5 μm and a typical dwell time of 0.8 s per step. Ninety-one line scans were measured, with the sample being rotated by 2°, yielding a 180° tomogram. Two fluorescence detectors (Vortex-60 EX/Vortex-90 EX; SII Nanotechnology USA) were used under 90° and 270° with respect to the incident beam to maximize detected fluorescence counts from the sample despite potential self-absorption while minimizing background (e.g. caused by elastic scattering due to the polarized nature of the synchrotron radiation).

The μ-XANES measurements were done at beamline P06 of the synchrotron PETRA III at the DESY. The x-ray beam was created in a 2m-undulator and monochromatized using a double-crystal monochromator in the range from 11,800 to 12,000 eV. In order to achieve good resolution, the energy was varied in steps of 0.5 eV in the XANES region, while step size was increased away from the edge to minimize beam damage to the sample. Focusing was achieved using Kirkpatrick-Baez mirrors to 0.8-μm spot size in both horizontal and vertical dimensions. The sample was cooled through a cryostream (Oxford Cryosystems) from the top to about 100 K. A polycapillary optic was used in front of the detector to only accept radiation from an approximately 130-μm-wide area of tissue along the axis of the beam. To select the tissues to be measured, a 2D map was first created and the positions of various tissues were observed (Fig. 2A). After having a good clean position for epidermis, mesophyll, and vein tissues, a fine sweep (Fig. 2B) was measured to select the exact measuring point in each tissue. Spectra were measured by monitoring the As Kα fluorescence using a Vortex-EM (SII Nanotechnology USA) detector at 90° to the incident beam. A gold foil was used for energy calibration. To improve the signal-to-noise ratio, up to nine scans were summed for tissues providing low count rates. To exclude tissue damage (e.g. beam-induced changes in oxidation state), for each of these scans the sample was moved by 2 μm along the axis of the leaf.

μ-XRF Data Analysis. The detected μ-XRF spectra were fitted using PyMca (Solé et al., 2007). The fluorescence line areas were then normalized to a 100-mA ring current, and the resulting sinograms were tomographically reconstructed with XRDUA (De Nolf and Janssens, 2010) using the maximum likelihood expectation maximization algorithm. Finally, the above-mentioned standard was used to relate fluorescence intensities with micromolar concentrations and to correct for matrix effects (Fig. 1, A–C). A histogram analysis was used to estimate the background level, which was then removed.

μ-XANES Data Analysis. The background of the spectra was removed, and normalization was done using the Athena program (version 0.8.056; by Bruce Ravel) as part of the IFEFFIT package (version 1.2.11; by Matt Newville). Afterward, in Microcal Origin Professional 8.1 (Originlab), the energy axis of all spectra was interpolated to the same sampling points in 0.5-eV steps. Quantitative analysis of near-edge spectra was carried out in SigmaPlot 11 (SPSS Science) by fitting to the sum of spectra of aqueous standard compounds along with a linear correction of background drift. Self-absorption effects on the fits were minimized by fitting for As(V) and As(III) both a spectrum measured in fluorescence mode and a spectrum measured in transmission mode; the spectra of As(III) and As(V) were kindly provided by Kirk Scheckel (personal communication). While spectra measured in transmission mode (which is only possible for highly concentrated samples) are free of quenching artifacts, the fluorescence excitation spectrum (as needed for low-concentration samples like our plant samples) is affected by self-absorption of the fluorescence inside the sample, and since geometry and concentrations in tissues cannot be kept exactly constant, fitting the contribution of self-absorption turned out to be the best option. However, in all plant samples, mostly the spectra measured in transmission mode contributed to the fits, showing that self-absorption in the plant samples was much weaker than in the standard.

Statistics

Usually, one-way ANOVA was done in SigmaPlot 11 (SPSS Science) at a significance level of $P = 0.05$. For significant effects, a posthoc all-pairwise comparison via the Student-Newman-Keuls method was performed. For As speciation through chromatography, two-way ANOVA was done and a posthoc all-pairwise comparison via the Holm-Sidak method was performed.

Supplemental Data

The following materials are available in the online version of this article.

Supplemental Figure S1. Growth parameters of plants exposed to different concentrations of As for 2 weeks.

Supplemental Figure S2. Speciation of As in plant extracts through anion-exchange chromatography coupled to ICP-MS.

Supplemental Figure S3. Fit quality of μ-XANES spectra of the epidermis of mature leaf, showing the linear combination fitting of standards as used in this study.

Supplemental Table S1. Composition of the nutrient solution.

ACKNOWLEDGMENTS

We thank HASYLAB/DESY for providing beam time, Karen Rickers, Manuela Borchert, and Björn De Samber for their help and support at beamline L and Gerald Falkenberg at beamline P06, and Dr. Kirk Scheckel for providing the spectra of As(III) and As(V).

Received July 2, 2013; accepted September 18, 2013; published September 20, 2013.

LITERATURE CITED

Asher CJ, Reay PF (1979) Arsenic uptake by barley seedlings. Aust J Plant Physiol **6:** 459–466

Bleeker PM, Hakvoort HWJ, Bliek M, Souer E, Schat H (2006) Enhanced arsenate reduction by a CDC25-like tyrosine phosphatase explains increased phytochelatin accumulation in arsenate-tolerant Holcus lanatus. Plant J **45:** 917–929

Bleeker PM, Schat H, Vooijs R, Verkleij JAC, Ernst WHO (2003) Mechanisms of arsenate tolerance in Cytisus striatus. New Phytol **157:** 33–38

Blüm V, Stretzke E, Kreuzberg K (1994) C.E.B.A.S.-AQUARACK project: the Mini-Module as tool in artificial ecosystem research. Acta Astronaut **33:** 167–177

Brammer H, Ravenscroft P (2009) Arsenic in groundwater: a threat to sustainable agriculture in South and South-east Asia. Environ Int **35:** 647–654

Cai Y, Su J, Ma LQ (2004) Low molecular weight thiols in arsenic hyperaccumulator Pteris vittata upon exposure to arsenic and other trace elements. Environ Pollut **129:** 69–78

Carey AM, Scheckel KG, Lombi E, Newville M, Choi Y, Norton GJ, Charnock JM, Feldmann J, Price AH, Meharg AA (2010) Grain unloading of arsenic species in rice. Plant Physiol **152:** 309–319

Carey AM, Norton GJ, Deacon C, Scheckel KG, Lombi E, Punshon T, Guerinot ML, Lanzirotti A, Newville M, Choi Y, Price AH, Meharg AA (2011) Phloem transport of arsenic species from flag leaf to grain during grain filling. New Phytol **192:** 87–98

Chowdhury UK, Biswas BK, Chowdhury TR, Samanta G, Mandal BK, Basu GC, Chanda CR, Lodh D, Saha KC, Mukherjee SK, Roy S, Kabir S, et al (2000) Groundwater arsenic contamination in Bangladesh and West Bengal, India. Environ Health Perspect **108:** 393–397

De Nolf W, Janssens K (2010) Micro x-ray diffraction and fluorescence tomography for the study of multilayered automotive paints. Surf Interface Anal **42:** 411–418

Duan GL, Zhu YG, Tong YP, Cai C, Kneer R (2005) Characterization of arsenate reductase in the extract of roots and fronds of Chinese brake fern, an arsenic hyperaccumulator. Plant Physiol **138:** 461–469

Hartley-Whitaker J, Ainsworth G, Vooijs R, Ten Bookum W, Schat H, Meharg AA (2001) Phytochelatins are involved in differential arsenate tolerance in *Holcus lanatus.* Plant Physiol **126:** 299–306

Hokura A, Omuma R, Terada Y, Kitajima N, Abe T, Saito H, Yoshida S, Nakai I (2006) Arsenic distribution and speciation in an arsenic hyperaccumulator fern by x-ray spectrometry utilizing a synchrotron radiation source. J Anal At Spectrom **21:** 321–328

Isayenkov SV, Maathuis FJM (2008) The Arabidopsis thaliana aquaglyceroporin AtNIP7;1 is a pathway for arsenite uptake. FEBS Lett **582:** 1625–1628

Keskinkan O, Goksu MZ, Basibuyuk M, Forster CF (2004) Heavy metal adsorption properties of a submerged aquatic plant (Ceratophyllum demersum). Bioresour Technol **92:** 197–200

Kopittke PM, de Jonge MD, Menzies NW, Wang P, Donner E, McKenna BA, Paterson D, Howard DL, Lombi E (2012) Examination of the distribution of arsenic in hydrated and fresh cowpea roots using two- and three-dimensional techniques. Plant Physiol **159:** 1149–1158

Küpper H, Küpper F, Spiller M (1996) Environmental relevance of heavy metal substituted chlorophylls using the example of submersed water plants. J Exp Bot **47:** 259–266

Küpper H, Lombi E, Zhao FJ, Wieshammer G, McGrath SP (2001) Cellular compartmentation of nickel in the hyperaccumulators Alyssum lesbiacum, Alyssum bertolonii and Thlaspi goesingense. J Exp Bot **52:** 2291–2300

Küpper H, Mijovilovich A, Meyer-Klaucke W, Kroneck PMH (2004) Tissue- and age-dependent differences in the complexation of cadmium and zinc in the cadmium/zinc hyperaccumulator *Thlaspi caerulescens* (Ganges ecotype) revealed by x-ray absorption spectroscopy. Plant Physiol **134:** 748–757

Küpper H, Zhao F, McGrath SP (1999) Cellular compartmentation of zinc in leaves of the hyperaccumulator *Thlaspi caerulescens*. Plant Physiol **119:** 305–311

Lombi E, Scheckel KG, Pallon J, Carey AM, Zhu YG, Meharg AA (2009) Speciation and distribution of arsenic and localization of nutrients in rice grains. New Phytol **184:** 193–201

Lombi E, Zhao FJ, Fuhrmann M, Ma LQ, McGrath SP (2002) Arsenic distribution and speciation in the fronds of the hyperaccumulator Pteris vittata. New Phytol **156:** 195–203

Ma JF, Yamaji N, Mitani N, Xu XY, Su YH, McGrath SP, Zhao FJ (2008) Transporters of arsenite in rice and their role in arsenic accumulation in rice grain. Proc Natl Acad Sci USA **105:** 9931–9935

Meharg AA, Lombi E, Williams PN, Scheckel KG, Feldmann J, Raab A, Zhu Y, Islam R (2008) Speciation and localization of arsenic in white and brown rice grains. Environ Sci Technol **42:** 1051–1057

Meharg AA, Macnair MR (1990) An altered phosphate uptake system in arsenate tolerant Holcus lanatus. New Phytol **116:** 29–35

Mishra S, Srivastava S, Dwivedi S, Tripathi RD (2013) Investigation of biochemical responses of Bacopa monnieri L. upon exposure to arsenate. Environ Toxicol **28:** 419–430

Mishra S, Srivastava S, Tripathi RD, Kumar R, Seth CS, Gupta DK (2006) Lead detoxification by coontail (Ceratophyllum demersum L.) involves induction of phytochelatins and antioxidant system in response to its accumulation. Chemosphere **65:** 1027–1039

Mishra S, Srivastava S, Tripathi RD, Trivedi PK (2008) Thiol metabolism and antioxidant systems complement each other during arsenate detoxification in Ceratophyllum demersum L. Aquat Toxicol **86:** 205–215

Mishra S, Tripathi RD, Srivastava S, Dwivedi S, Trivedi PK, Dhankher OP, Khare A (2009) Thiol metabolism play significant role during cadmium detoxification by Ceratophyllum demersum L. Bioresour Technol **100:** 2155–2161

Moore KL, Schröder M, Lombi E, Zhao FJ, McGrath SP, Hawkesford MJ, Shewry PR, Grovenor CR (2010) NanoSIMS analysis of arsenic and selenium in cereal grain. New Phytol **185:** 434–445

Moore KL, Schröder M, Wu Z, Martin BG, Hawes CR, McGrath SP, Hawkesford MJ, Feng Ma J, Zhao FJ, Grovenor CR (2011) High-resolution secondary ion mass spectrometry reveals the contrasting subcellular distribution of arsenic and silicon in rice roots. Plant Physiol **156:** 913–924

Ohno K, Yanase T, Matsuo Y, Kimura T, Rahman MH, Magara Y, Matsui Y (2007) Arsenic intake via water and food by a population living in an arsenic-affected area of Bangladesh. Sci Total Environ **381:** 68–76

Panaullah GM, Alam T, Hossain MB, Loeppert RH, Lauren JG, Meisner CA, Ahmed ZU, Duxbury JM (2009) Arsenic toxicity to rice (Oryza sativa L.) in Bangladesh. Plant Soil **317:** 31–39

Parsons JG, Aldrich MV, Gardea-Torresdey JL (2002) Environmental and biological applications of extended x-ray absorption fine structure (EXAFS) and x-ray absorption near edge structure (XANES) spectroscopies. Appl Spectrosc Rev **37:** 187–222

Pickering IJ, Gumaelius L, Harris HH, Prince RC, Hirsch G, Banks JA, Salt DE, George GN (2006) Localizing the biochemical transformations of arsenate in a hyperaccumulating fern. Environ Sci Technol **40:** 5010–5014

Pickering IJ, Prince RC, George MJ, Smith RD, George GN, Salt DE (2000) Reduction and coordination of arsenic in Indian mustard. Plant Physiol **122:** 1171–1177

Raab A, Feldmann J, Meharg AA (2004) The nature of arsenic-phytochelatin complexes in *Holcus lanatus* and *Pteris cretica.* Plant Physiol **134:** 1113–1122

Raab A, Schat H, Meharg AA, Feldmann J (2005) Uptake, translocation and transformation of arsenate and arsenite in sunflower (Helianthus

annuus): formation of arsenic-phytochelatin complexes during exposure to high arsenic concentrations. New Phytol **168:** 551–558

Salt DE, Prince RC, Pickering IJ, Raskin I (1995) Mechanisms of cadmium mobility and accumulation in Indian mustard. Plant Physiol **109:** 1427–1433

Schmöger MEV, Oven M, Grill E (2000) Detoxification of arsenic by phytochelatins in plants. Plant Physiol **122:** 793–801

Smedley PL, Kinniburgh DG (2002) A review of the source, behaviour and distribution of arsenic in natural waters. Appl Geochem **17:** 517–568

Smith PG, Koch I, Gordon RA, Mandoli DF, Chapman BD, Reimer KJ (2005) X-ray absorption near-edge structure analysis of arsenic species for application to biological environmental samples. Environ Sci Technol **39:** 248–254

Sneller FEC, van Heerwaarden LM, Kraaijeveld-Smit FJL, Ten Bookum WM, Koevoets PLM, Schat H, Verkleij JAC (1999) Toxicity of arsenate in Silene vulgaris, accumulation and degradation of arsenate-induced phytochelatins. New Phytol **144:** 223–232

Solé VA, Papillon E, Cotte M, Walter P, Susini J (2007) A multiplatform code for the analysis of energy-dispersive x-ray fluorescence spectra. Spectrochim Acta B At Spectrosc **62:** 63–68

Song WY, Park J, Mendoza-Cózatl DG, Suter-Grotemeyer M, Shim D, Hörtensteiner S, Geisler M, Weder B, Rea PA, Rentsch D, Schroeder JI, Lee Y, et al (2010) Arsenic tolerance in Arabidopsis is mediated by two ABCC-type phytochelatin transporters. Proc Natl Acad Sci USA **107:** 21187–21192

Srivastava S, Mishra S, Tripathi RD, Dwivedi S, Trivedi PK, Tandon PK (2007) Phytochelatins and antioxidant systems respond differentially during arsenite and arsenate stress in Hydrilla verticillata (L.f.) Royle. Environ Sci Technol **41:** 2930–2936

Tripathi RD, Srivastava S, Mishra S, Singh N, Tuli R, Gupta DK, Maathuis FJ (2007) Arsenic hazards: strategies for tolerance and remediation by plants. Trends Biotechnol **25:** 158–165

Webb SM, Gaillard JF, Ma LQ, Tu C (2003) XAS speciation of arsenic in a hyper-accumulating fern. Environ Sci Technol **37:** 754–760

Xu XY, McGrath SP, Zhao FJ (2007) Rapid reduction of arsenate in the medium mediated by plant roots. New Phytol **176:** 590–599

Xue P, Yan C, Sun G, Luo Z (2012) Arsenic accumulation and speciation in the submerged macrophyte Ceratophyllum demersum L. Environ Sci Pollut Res Int **19:** 3969–3976

Zhao FJ, Wang JR, Barker JHA, Schat H, Bleeker PM, McGrath SP (2003) The role of phytochelatins in arsenic tolerance in the hyperaccumulator Pteris vittata. New Phytol **159:** 403–410